Multiyear Predictability of Northern Hemisphere Surface Air Temperature in the Kiel Climate Model

Y. Wu[1,2], M. Latif[1,2], and W. Park[1]

[1]GEOMAR Helmholtz Centre for Ocean Research Kiel, Kiel, Germany

[2]University of Kiel, Kiel, Germany

Abstract

The multiyear predictability of Northern Hemisphere surface air temperature (SAT) is examined in a multi-millennial control integration of the Kiel Climate Model (KCM), a coupled ocean-atmosphere-sea ice general circulation model. A statistical method maximizing Average Predictability Time (APT) is used to identify the most predictable SAT patterns in the model. The two leading APT modes are much localized and the physics are discussed that give rise to the enhanced predictability of SAT in these limited regions. Multiyear SAT predictability exists near the sea ice margin in the North Atlantic and mid-latitude North Pacific sector. Enhanced predictability in the North Atlantic is linked to the Atlantic Multidecadal Oscillation (AMO) and to the sea ice changes. In the North Pacific, the most predictable SAT pattern is characterized by a zonal band in the western and central mid-latitude Pacific. This pattern is linked to the Pacific Decadal Oscillation (PDO), which drives sea surface temperature (SST) anomalies. The temperature anomalies subduct into deeper ocean layers and re-emerge at the sea surface during the following winters, providing multiyear memory. Results obtained from the Coupled Model Intercomparison Project Phase 5 (CMIP5) ensemble yield similar APT modes. Overall, the results stress the importance of ocean dynamics in enhancing predictability in the atmosphere.

1. Introduction

The climate system shows wide range of variability that arises from interactions within and between different components of the Earth system. Predictable time scales of the variability differ in each component. In general, internally generated atmospheric variability, i.e. weather, loses memory within less than a month (Lorenz, 1963). However, a large number of studies support the existence of potentially predictable variations in the atmosphere on multiyear time scale (Boer and Lambert, 2008; Collins et al., 2006; Meehl et al., 2009; DelSole et al., 2013). Therefore, beyond time scales of a month, the atmospheric predictability should arise from forcing by the slowly varying boundary conditions such as changes in sea surface temperature (SST), soil moisture, or sea ice. Latif et al. (2006) reviewed different approaches of estimating multiyear to decadal SAT predictability and found all approaches indicate four regions with enhanced predictability and where long-term SAT variations are related to ocean dynamics: the North Atlantic, the North Pacific, the tropical Pacific, and the Southern Ocean. In the North Atlantic, the multidecdal SST variability, which is referred to as the Atlantic Multidecadal Oscillation (AMO; Kerr, 2000), is assumed, based on climate model simulations, to be driven by variations of the Atlantic Meridional Overturning Circulation (AMOC) through northward heat transport (Delworth et al., 1993; Knight et al., 2005; Yang et al., 2013). There is evidence that SST and SAT variations associated with the AMOC are potentially predictable on multiyear or even decadal time scale (Collins et al., 2006; Pohlmann et al, 2006; Branstator et al., 2012; Branstator and Teng, 2014). In the North Pacific, the predictability of SAT is lower than in the North Atlantic, but still in on the multiyear time scale (Branstator et al, 2012; DelSole et al., 2013). In the tropical Pacific, it is mostly the off-equatorial region that exhibits multiyear SAT predictability, whereas the equatorial Pacific depicts strong predictability on seasonal to annual but not on multiyear time scale. Finally, the Southern Ocean depicts a rather long predictability potential, in some climate models even at the multidecadal time scale, but the processes are poorly understood and strongly vary from model to model. Here we concentrate on the Northern Hemisphere.

There are two distinct classes of predictability (Lorenz, 1975): The predictability associated with initial conditions is referred to as predictability of the first kind, whereas that associated with the slowly evolving boundary conditions or external forcing, e.g., SST, anthropogenic forcing and volcanic eruptions, is defined as predictability of the second kind. On multiyear time scale, both factors could influence predictability (Meehl et al., 2009). DelSole and Teppett (2009a, b) proposed a method to optimize predictability integrated over all time lags and find maximizing predictable pattern. This approach is called Average Predictability Time (APT). Using this method, previous studies exhibit multiyear predictability of SAT in the North Atlantic and North Pacific with model ensemble data and observations (DelSole et al., 2013; Jia and DelSole, 2013). Here we focus on understanding the underlying mechanism giving rise to the enhanced predictability in the localized regions yielded by the APT method. For example, it is well known that the pattern associated with the AMO, a pattern covering the whole North Atlantic poleward of the Equator, exhibits enhanced predictability. But which part of that basin-scale pattern is the most predictable, and why? What are the relevant processes?

This study is organized as follow. We briefly describe in section 2 the Kiel Climate Model used, the multi-model ensemble from CMIP5 and the reanalysis data. Section 3 describes the APT method and potential predictability variance fraction approach. In section 4, we present global patterns of potential predictability and explore the mechanisms that give rise to multiyear predictability in the North Atlantic and North Pacific. The paper finishes with a discussion of the results and conclusions that can be drawn from this study.

2. Model and data

We analyze data obtained from a control integration of the Kiel Climate Model (KCM; Park et al., 2009). The KCM consists of the ECHAM5 atmosphere model (Roeckner et al., 2003) and NEMO ocean-ice coupled model (Madec, 2008). The resolution of the atmospheric component is horizontally T31 (about 3.75°) with 19 vertical levels. The ocean component runs on a 2° Mercator mesh, with 1.3° horizontal resolution on average, but in the equatorial region it increases to 0.5° in the meridional direction. The ocean model uses 31 vertical levels. The KCM runs with no form of flux correction or anomaly coupling. The control run is about 5,000 years long and employs constant "present-day" CO_2-concentration of 348 ppmv. In this study, the last 4,200 years is used to reduce effects of model spin-up. We use annual mean data, unless stated otherwise.

We also use data of control runs from 17 CMIP5 models (Taylor et al., 2012; Table 1). In contrast to the KCM, these are pre-industrial control integrations. There is a residual warming trend in globally averaged SAT of about 0.001 °C/100yrs in the KCM. However, this trend is not significant and within the range of trends calculated from the CMIP5 models amounting to 0.014±0.03 °C/100yrs. Moreover, although the trend in the KCM is small, we removed it before conducting the predictability analyses. This was also done in the CMIP5 analyses. Following Boer (2004), trends have been removed by subtracting a third-order polynomial at each grid point. The results are not sensitive to the order of the polynomial. The CMIP5 data are interpolated on a common 3°×3° resolution grid. Again, analyses are performed on annual-mean SATs, and for each model, only the last 300 years of the simulations is used. The data are concatenated to a 5,100-year long multi-model time series which enters the APT method.

We also use detrended 2-meter air temperature from 20th century reanalysis (20CR) V2 data from 1871 to 2012 (Compo et al., 2012). We use two SST indices in Fig. 10. First, the AMO index defined as the detrended, area-weighted average SST anomalies over the North Atlantic 0°-70°N taken from the Kaplan SST dataset (Kaplan et al., 1998; Enfield et al., 2001; http://www.esrl.noaa.gov/psd/data/timeseries/AMO/). Second, the PDO index derived from the leading Principal Component (PC) of North Pacific SST anomalies poleward of 20°N (Mantua et al. 1997; http://research.jisao.washington.edu/pdo/PDO.latest). We calculate the AMO and PDO indices in the KCM and CMIP5 ensemble following the same definitions.

3. Methods

We applied two approaches to estimate multiyear predictability in this study. First, potential predictability variance fraction (ppvf) provides general information about the fraction of slowing varying variability with respect to the total variability, i.e. potential predictability. Second, we computed the most predictable modes with the Average Predictability Time (APT) method.

3.1 Potential predictability

The potential predictability variance fraction proposed by Boer (2004) attempts to decompose variance into a long timescale part and an unpredictable "noise" part. It assumes that climate variability could be represented in the form $X=\nu+\varepsilon$, where ν is the slow long timescale variability and ε is the remaining unpredictable noise with variance $\sigma^2=\sigma_\nu^2+\sigma_\varepsilon^2$. The potential predictability variance fraction is $p=\sigma_\nu^2/\sigma^2$, which is a kind of normalized signal variance. The deterministic long timescale variability that arises above the noise is presumed at least *potentially predictable*.

3.2 Average Predictability Time

For univariate cases, a standard measure of predictability is

$$P(\tau) = 1 - \frac{\sigma_\tau^2}{\sigma_\infty^2}, \qquad (1)$$

where σ_τ^2 is the forecast error variance at lead time τ given by the square of the difference between the predicted and "observed" state, and σ_∞^2 the climatological variance. In the APT method, predictability arises from the Mahalanobis signals (DelSole and Tippett, 2007). In principle, predictability is a function of the lead time τ and decays monotonically from 1 to 0. DelSole and Tippett (2009a, b) proposed the Average Predictability Time (APT) method. APT is defined as the integral of predictability over all lead times, which can be written as

$$\mathrm{APT} = 2\sum_{\tau=1}^{\infty}\left(1-\frac{\sigma_\tau^2}{\sigma_\infty^2}\right). \tag{2}$$

Therefore, it is independent of the lead time and characterizes an integral property of the climate system. In this method, a linear regression model is used for forecast to estimate error variance in (2). The prediction model is in the form of $\hat{y}_{(t+\tau)}=L_\tau x_{(t)}$, where $x_{(t)}$ is the predictor, $\hat{y}_{(t+\tau)}$ the predicted value, and L_τ is the regression operator at lead time τ obtained from the least squares method. Thus, predictability arising from nonlinear processes will be missed. Following DelSole and Tippett (2009a), for multivariate cases, maximizing APT could be solved by a generalized eigenvalue problem

$$\left(2\sum_{\tau=1}^{\infty}C_{yx}C_{xx}^{-1}C_{yx}^{T}\right)q = \lambda C_{yy}q, \tag{3}$$

where C is the covariance matrix. The term in the bracket on the left-hand is the integration of signal covariance, C_{yy} is the total covariance of the predictand, and q is a projection vector. The eigenvalue λ in equation (3) gives the value of APT associated with each eigenvector. Like EOF analysis, we can obtain a set of orthogonal components ordered according to predictability time λ. The APT method is comparable to EOFs, except decomposing predictability instead of variance. More details can be found in DelSole and Tippett (2009b).

In practice, the predictors and the predictands are projected on the leading PCs to reduce the spatial dimensions. The sensitivity of the APTs to the number of PCs and lead times has been estimated by varying the numbers, but the major results are not very sensitive. We decided to use 40 PCs accounting for 84% and 81% of the total variance in the KCM and CMIP5 data, respectively. The maximum lead time is 20 years. The significance of the APTs is tested by a Monte Carlo method which is described in detail in Jia and DelSole (2011).

4. Results

We first show the climatology of selected variables as simulated by the KCM. The barotropic streamfunction shows the well-known features of the general ocean circulation depicting, for example, the wind-driven gyres and the Antarctic Circumpolar Current (Fig. 1a). In the North Atlantic, however, the streamfunction is too zonal, indicating a poor representation of the Northwest Corner, which is a common problem in low-resolution climate and ocean models. The AMOC, an important part of global thermohalince circulation, is shown by the overturning streamfunction. The mean AMOC strength is about 14 Sv (1Sv=$10^6 m^3/s$) at 30°N (Fig. 1b), which is somewhat weaker than that suggested by observations (Lumpkin and Speer, 2003; Cunningham et al., 2007). Park and Latif (2008) describe the internal AMOC variability showing a rich spectrum of variations from interannual, through decadal to multi-centennial time scales. They used the same simulation that is used here and concluded that the multidecadal variability of AMOC is controlled by North Atlantic processes, while multi-centennial AMOC variability by Southern Hemisphere processes. Deep convection in the North Atlantic occurs south of Greenland, in the Irminger Sea and Greenland-Iceland-Norwegian (GIN) Sea (Fig. 1c), which all contribute to the formation of North Atlantic Deep Water. In the Southern Ocean, the deep convection associated with the formation of the Antarctic Bottom Water is found in the Weddell Sea, with an annual-mean mixed layer depth

(MLD) of about 1,300 meters. The MLD is also relatively deep in the mid-latitude North Atlantic and North Pacific, which is related to the intermediate water formation there. The annual-mean Arctic sea ice area is about $12 \cdot 10^6$ km^2, which is slightly larger than the observed estimate of $11.3 \cdot 10^6$ km^2 from 1960-1990 (Rayner et al., 2003). Due to larger sea ice extent, the deep convection in the Labrador Sea is shifted to the open ocean to south of Greenland (Fig. 1d).

4.1 Global potential predictability

We estimate the potential predictability (see section 3.1) using pentadal, decadal and 25-year means of surface air temperature (SAT) from both the KCM and the CMIP5 ensemble (Fig. 2). Low-latitude regions display relatively low potential predictability when compared to mid- and high latitudes, which is consistent with earlier studies using CMIP3 simulations (Boer and Lambert, 2008; Boer, 2009). This tendency becomes more obvious as the time scale increases: when considering 25-year means of SAT (bottom panels), potential predictability variance is mainly concentrated in the North Atlantic, the mid-latitude North Pacific, and the Southern Ocean. In general, potential predictability signals are stronger in the KCM than that obtained from the CMIP5 models. The larger values of ppvf in the KCM indicate that the long timescale variability is more pronounced compared to that with the CMIP5 ensemble. This may be due to the large model-to-model differences in the CMIP5 ensemble that introduces "noise". Also, it is possible that the KCM simulates more long-timescale variability than the CMIP5 models. The most robust differences in both datasets are in the Southern Ocean, which may arise from the pronounced centennial to multi-centennial scale variability in the KCM

(Park and Latif, 2008; Latif et al., 2013; Martin et al., 2013) and CMIP5 models. The intention behind the comparison shown in Figure 2 is not to investigate the detailed differences between the KCM and the CMIP5 models, but to indicate that essential features of potential predictability obtained from the CMIP5 models are also observed in the KCM. In the following, we focus on the Northern Hemisphere and discuss predictability only in the KCM.

4.2 APT1

The most predictable component (APT1) in the Northern Hemisphere SAT in the KCM depicts significant positive loadings along the sea ice margin in the North Atlantic, with maximum loadings extending from Southern Greenland to the northeast into the Barents Sea (Fig. 3a). Downstream signals over land areas are generally weak, with the exception of Scandinavia. These signals have been also described in some previous studies, although these studies conducted APT analysis on global SAT (Jia and DelSole, 2013; Yang et al., 2013). The value for APT1 in the KCM is 8.6 years. In general, the APT value is related to the decay time scale of the corresponding predictable mode, and larger APT values represent systems with less damping that hence are more predictable. The corresponding time series of APT1 shows pronounced multi-decadal fluctuations with a very strong spectral peak at a period of about 60 years (Figs. 3b, c). Obviously, the APT method is time scale-selective and acts as a kind of band-pass filter on the SAT variability which exhibits a red-noise character. The APT1 mode is highly correlated with the model's AMO mode which exhibits a peak at the same period (Park and Latif, 2010; Ba et al., 2014). What is important here is that not all components of the AMO pattern are equally predictable, but that instead it is the region in the vicinity of the sea ice margin that exhibits the largest SAT predictability potential.

In order to understand the processes related to the leading APT modes, we conduct a heat budget analysis of the upper North Atlantic:

$$\frac{\partial Q}{\partial t} = Q_{net} + \rho c_p \int_{-H}^{0} \left(-u\frac{\partial T}{\partial x} - v\frac{\partial T}{\partial y} - w\frac{\partial T}{\partial z}\right) dz + Q_{res} \qquad (4).$$

Here Q is the vertically integrated heat storage, Q_{net} the net heat flux, the integral on the right-hand side the ocean heat flux convergence, Q_{res} the residual part presenting unresolved sub-grid scale and sub-annual processes, and H the layer thickness of 273 meters. For annual-mean data, the tendency of Q is generally small and not shown here.

We perform composite analysis on North Atlantic SST, net surface heat flux and ocean heat flux convergence using one (plus and minus) standard deviation of the APT1 time series (see red dashed lines Fig. 3b) as thresholds. The SST composite, shown as the difference between the two polarities (Fig. 4a), is, as expected, similar to the APT1 pattern (Fig. 3a), with positive anomalies over the Irminger Sea and GIN Sea. The positive ocean heat flux convergence anomalies in these regions suggest that the warm SST anomalies are caused by ocean dynamics (Fig. 4b). In fact the net surface heat flux anomalies are negative, indicating the ocean loses heat to the atmosphere (Fig. 4c). This confirms that the anomalous warm SATs in the pattern of APT1 (Fig. 3a) are indeed driven by the ocean. The contribution of the residual part to the heat budget is relatively small (Fig. 4d). Our findings with the KCM are consistent with those of DelSole et al. (2013). They obtained a similar mode, but derived from SST, from the analysis of the CMIP5 models, and that mode is also closely related to the models' AMO. Again consistent with the KCM results, the APT pattern from the CMIP5 models is much more localized than the AMO patterns themselves.

To further understand the differences between the patterns of the AMO and APT1 in the KCM, we compute composites of barotropic stream function and sea ice concentration anomalies (Fig. 5) with respect to the APT1 time series. In comparison to the long-term mean of the barotropic stream function (Fig. 1a), the composite anomaly (Fig. 5a) indicates an intensification of the subtropical and subpolar gyre, and North Atlantic Current transporting more warm water into the Irminger Sea, Greenland Sea and Barents Sea. The intrusion of the anomalously warm water leads to sea ice melt (Fig. 5b). This process locally accounts for more than 40% of the explained variance in the sea ice concentration variability (not shown), which was derived from regression analysis with the APT1 time series. The changes of ice cover in the region of the sea ice margin produce large changes in the net heat flux at the air-sea interface (Fig. 4c). This results in a higher signal-to-noise ratio, which is eventually presented in the potential predictability pattern (Fig. 2). It is the positive feedback by the sea ice that explains the localized APT1 pattern in comparison to that of the AMO in the KCM. In conclusion, the sea ice response is a key to provide largest multiyear predictability in the subpolar North Atlantic region.

4.3 APT2

The second most predictable component, APT2, of Northern Hemisphere SAT in the KCM has an APT value amounting to 7.2 years. Its pattern is characterized by negative SAT anomalies in the mid-latitude North Pacific (Fig. 6a). The potential predictability analysis discussed above also implies enhanced predictability in this area (Fig. 2). As for APT1, loadings over land are virtually absent. The spectrum of the APT2 time series (Fig. 6b) exhibits peaks at a period of about 30 years and a century, and also depicts enhanced power at multi-centennial time scales (Figs. 6c). The origin of the centennial and multi-centennial peaks is not well understood. They could be due to the influence of long-term variability in the Southern Ocean (Latif et al. 2013, Martin et al. 2013). Further, the potential predictability analysis described above, based on the 25-year means of SAT, indicates a rather long predictability potential in the North Pacific on the multidecadal and centennial time scale (bottom left panel of Fig. 2). The issue of basin-basin interactions on these long time scales will be the subject of further investigations and is not discussed here.

We concentrate in the following only on the North Pacific. The corresponding SST anomaly composite (Fig. 7a) shows a band of negative SST anomalies in the mid-latitude North Pacific. From the heat budget analysis, it can be inferred that, as in the APT1, the ocean dynamics drive the SST anomalies, as a strong negative heat flux convergence anomaly, i.e. heat flux divergence anomaly, is seen in the center of the negative SST anomaly (Figs. 7b). As the SST cools, less heat is transferred from ocean to the atmosphere (Fig. 7c), indicating that the atmosphere damps the SST anomalies there. Like in the APT1, the contribution of the residual part is rather small (Fig. 7d).

The APT2 mode found in the KCM shows a connection to the PDO, consistent with previous studies (DelSole et al., 2013). Its time series (Fig. 6b) is correlated with the model’s PDO index at about 0.5, when the PDO index leads by 2 to 3 years. This suggests that the PDO drives the APT2 mode in some way. However, the SST anomaly composite associated with the APT2 time series is markedly different from the PDO pattern. The latter is characterized by SST anomalies of one sign in the western and central mid-latitude Pacific that are surrounded by SST anomalies of opposite signs (Mantua et al., 1997). In contrast, the APT2 SST anomaly composite (Fig. 7a) is concentrated in a rather narrow region in the western and central Pacific where it has strong loadings of only one polarity. To investigate the physical process associated with APT2, we perform cross-correlation analysis of monthly vertical ocean temperature anomalies averaged over the central and western Pacific (145°-165°E, 40°-45°N) with the (annual) APT2 time series (Fig. 8). The most robust link is seen in winter when APT2 of SAT lags ocean temperatures by 2 years. The negative SST anomalies in this region and at that lead time are related to the positive PDO-index phase and very likely heat flux-driven. The SST anomalies are subducted into subsurface layers in winter and preserved under the seasonal thermocline in summer. The cold temperature anomalies reemerge at the surface during the following winters in response to strong vertical mixing (Alexander and Deser, 1995; Alexander et al., 1999). It is this ocean memory that eventually provides the enhanced predictability of the North Pacific SAT. The maximum mixed layer depth increases from east to west during winter, while the mixed layer shoals to similar depth during summer. The vertical extent of temperature anomalies below the mixed layer is therefore greater in the west than the east (Alexander and Deser, 1995), with the consequence that the reemergence mechanism is more effective in the western and central Pacific.

4.4 CMIP5 model ensemble results

In order to investigate the sensitivity of the results obtained from the KCM to model formulation, we also computed the most predictable components from the CMIP5 multi-model ensemble. For consistency, we conduct the analysis only for Northern Hemisphere SAT, whereas previous studies have used global SAT. The most predictable APT mode from the CMIP5 ensemble has signals concentrated along the sea ice margin in the North Atlantic sector (Fig. 9a), which is similar to APT1 calculated from the KCM (Fig. 3a). The APT1 value from CMIP5 is 5.6 year, as opposed to 8.6 years in the KCM. The leading APT mode from CMIP5 is correlated with the (concatenated) AMO index at 0.54, suggesting a significant link to the AMO. The changes in sea ice concentrations are consistent with those in the KCM and concentrated near the sea ice margin, but somewhat weaker (not shown). Overall, the leading APT mode from CMIP5 is in line with that in the KCM.

The second most predictable mode derived from the CMIP5 ensemble is also consistent with APT2 from the KCM (Fig. 9b). The corresponding APT value is 5.0 years, as opposed to 7.2 years in the KCM. The correlation with the (concatenated) PDO index amounts to 0.67 with no lag. Although a signal is seen in the eastern North Pacific, the most significant loadings are in the west and central mid-latitude part of the basin. Thus, we conclude that the two leading APT modes from the CMIP5 ensemble support the KCM results, with the caveat that the lead-lag relationship between the PDO index and the APT2 time series is different.

5. Discussion

We have investigated, by means of the Average Predictability Time (APT) method, the predictability of Northern Hemisphere surface air temperature (SAT) from a control integration of the Kiel Climate Model (KCM). We have discussed the two leading APT modes, APT1 and APT2, from the KCM and compared them with the two leading APT modes computed from the CMIP5 database. We find the leading modes obtained from the KCM and CMIP5 data are consistent with each other. In the KCM, the pattern of APT1 is localized in the North Atlantic along the sea ice margin. This mode is connected to the Atlantic Multidecadal Oscillation (AMO) and driven by ocean dynamics. Sea ice provides an important positive feedback on SAT. The second most energetic APT mode, APT2, from the KCM has strongest loadings in the western and central mid-latitude North Pacific. It is linked to the Pacific Decadal Oscillation (PDO) which drives the APT mode in the first place. However, enhanced predictability is due to the reemergence mechanism, which makes the APT2 pattern rather localized and is the reason that APT2 correlates with the PDO index with a lag of 2 to 3 years. Neither of the aforementioned studies discussed the discrepancy between the highly localized APT patterns of SAT and the basin-scale SST variability patterns, the AMO and PDO.

The APT values of the leading two modes are smaller than the intrinsic time scale of the patterns. In fact, the spectra of the APT time series exhibit peaks at decadal and even centennial time scales. This is due to the fact that predictability as defined above is more related to the decay time scale rather than the variability time scale. We computed the efolding time from the APT1 and APT2 time series, and they amount to about 7 and 5 years, respectively, in the KCM, and they are even shorter in the CMIP5 ensemble, which is also reflected in the shorter the ATP values. In summary, the APT analyses suggest that the decadal modes identified in SAT are strongly damped and their predictability rather limited.

We obtained here multiyear predictability in the northern North Atlantic (APT1), which to some extent is consistent with that described in previous studies (Boer 2004; Latif et al., 2006; Yang et al., 2013). In this study, we connected the discrepancy between the APT1 pattern and the AMO pattern to sea ice in the North Atlantic. As the sea ice cover changes due to changes in oceanic heat transport, the net heat flux into the atmosphere may also change dramatically (Figs. 4, 5). Previous studies support the important role of sea ice changes due to SST changes in the North Atlantic and indicated that the associated modification in heat flux could have a strong impact on the atmosphere (Deser et al., 2004; Van der Swaluw et al., 2007). Thus, the slowly-varying part of the surface air temperature, which is usually driven from the ocean and sea ice, can, through the positive sea ice feedback, increase relative to the unforced atmospheric background spectrum. This suggests an importance role of sea ice in predicting surface air temperature in the North Atlantic sector on multiyear timescale.

The second most energetic APT mode (APT2) is concentrated in the North Pacific. The PDO and the reemergence process play an important role in APT2. The PDO drives temperature anomalies at the surface; these subduct and reemerge during the subsequent winters. Thus, the regions with oceanic reemergence have high predictability. Previous studies have suggested that in the North Pacific, SST persistence is associated with the thermal inertia of the mixed layer, which can be several years due to the reemergence mechanism (Alexander and Deser, 1995; Deser et al. 2003). Through surface heat flux, this may also give rise to the enhanced predictability of surface air temperature in this region. Thus, the APT2 mode is not concurrent with the PDO in the KCM, but lags the PDO by 2 to 3 years. However, this is not the case for the APT2 from the CMIP5 models, which depicts a simultaneous link to the PDO index. The origin of this discrepancy is unknown, but it may due to large model-to-model variations and also the short length of each model output (only 300 years).

As pointed out above, long-timescale (multidecadal to centennial) SAT predictability is found in the mid- and high-latitude Southern Ocean, in both the KCM and the CMIP5 models, where SAT variability is strongly linked to the abyssal ocean by deep convection (Martin et al. 2013).

The length of integration required to obtain stable results is also investigated with the KCM. We find that an integration of 1,000 years is not long enough for the APT analysis (not shown). Further, we performed APT analysis on several individual CMIP5 models and the results were different to those when using the concatenated SATs from all models (Fig. 9), supporting the need for long integration times. This is due to the influences of centennial to multi-centennial variability simulated by a number of climate models (e.g., Park and Latif, 2008; Delworth and Feng, 2012; Latif et al., 2013; Martin et al., 2013). Yet the essential features derived from the very long integration of the KCM are also seen in the results obtained from the concatenated CMIP5 SATs (Fig. 2 and Fig. 9). This suggests that by simply concatenating the time series of many models with relatively short integration times may be useful to reduce uncertainties.

Since the above results are only based on climate models, following DelSole et al. (2013), we projected the detrended SATs from 20CR onto the leading two predictable modes (APT1 and APT2) of the KCM (Fig. 10). The projections exhibit similar multidecadal variations as those seen in the observed AMO index (correlation 0.68) and PDO index (correlation 0.40), indicating some consistency of the most predictable modes in the KCM with observed decadal climate modes.

6. Conclusions

We have examined the multiyear predictability of Northern Hemisphere surface air temperature (SAT) and the underlying mechanisms, giving rise to the enhanced predictability in localized regions. To this end we investigated a multi-millennial control integration of the Kiel Climate Model (KCM), a coupled atmosphere-ocean-sea ice general circulation model, and a number of multi-century (pre-industrial) control integrations obtained from the CMIP5 climate model ensemble. The most robust signals of multiyear SAT predictability are found in the North Atlantic and North Pacific sectors. Predictability over land areas is found to be limited to rather small regions. The most predictable pattern is closely related to the AMO, with significant signals in the sea ice margin region of the North Atlantic where positive sea ice feedback provides enhanced localized predictability of SAT. This pattern locally explains up to 40% of the SAT variance computed from annual means. The leading APT mode derived from the CMIP5 ensemble is in good agreement with that of the KCM.

The second most predictable pattern in the KCM is concentrated in the mid-latitude North Pacific and related to the PDO, with the reemergence mechanism providing the multiyear memory. This mode locally accounts for up to 30% of the SAT variance (computed from annual-means) in that region. The region of enhanced SAT predictability in the North Pacific is consistent with that depicted by APT2 calculated from the CMIP5 models. However, the reemergence mechanism is not obvious when considering all CMIP5 models together, which does not exclude that it operates in some of the CMIP5 models.

Due to the lack of sufficient observations, multiyear predictability studies are heavily relying on climate models. However, state-of-art climate models suffer from large biases (Flato et al., 2013; Wang et al., 2014). In particular the simulation of SSTs in the North Atlantic and North Pacific is flawed, with cold SST biases typically on the order of several centigrade. It thus remains unclear how much of the results presented here carry over to the real world. Yet some consistency has been demonstrated between the models results and observed climate modes. This investigation suggests regions of enhanced multiyear SAT predictability in the Northern Hemisphere, and it is the processes in these regions that may deserve special attention in observational and modeling studies concerned with decadal variability and multiyear predictability.

Acknowledgement

We thank Liwei Jia in the Center for Ocean-Land-Atmosphere Studies (USA) for E-mail discussion about the APT method and Thomas Martin at GEOMAR for downloading the

CMIP5 data. Y. Wu was financially supported by the China Scholarship Council (CSC). The work was also supported by the BMBF-RACE (No. 03F0651B) and EU-NACLIM (grant agreement No. 308299) projects. The KCM model integrations were conducted at the Computer Center of Kiel University.

References

Alexander, M. A., and C. Deser, 1995: A Mechanism for the Recurrence of Wintertime Midlatitude SST Anomalies. *J. Phys. Oceanogr.*, 25, 122–137.doi: http://dx.doi.org/10.1175/1520-0485(1995)025<0122:AMFTRO>2.0.CO;2.

Alexander, M. A., C. Deser, and M. S. Timlin, 1999: The Reemergence of SST Anomalies in the North Pacific Ocean. *J. Climate*, 12, 2419–2433. doi: http://dx.doi.org/10.1175/1520-0442(1999)012<2419:TROSAI>2.0.CO;2.

Ba, J., and Coauthors, 2014: A multi-model comparison of Atlantic multidecadal variability. *Clim. Dyn.*, **43**, 2333–2348, doi:10.1007/s00382-014-2056-1.

Boer, G. J., 2004: Long time-scale potential predictability in an ensemble of coupled climate models. *Clim. Dyn.*, 23, 29-44. doi: 10.1007/s00382-004-0419-8.

Boer, G. J., and S. J. Lambert, 2008: Multi-model decadal potential predictability of precipitation and temperature. *Geophys. Res. Lett.*, 35, L05706, doi:10.1029/2008GL033234.

Boer, G. J., 2009: Changes in Interannual Variability and Decadal Potential Predictability under Global Warming. *J. Climate*, 22, 3098–3109. doi:

http://dx.doi.org/10.1175/2008JCLI2835.1.

Branstator, G., H. Teng, G. A. Meehl, et al., 2012: Systematic Estimates of Initial-Value Decadal Predictability for Six AOGCMs. *J. Climate*, 25, 1827–1846. doi: http://dx.doi.org/10.1175/JCLI-D-11-00227.1.

Branstator, G., and H. Teng, 2014: Is AMOC More Predictable than North Atlantic Heat Content? *J. Climate*, 27, 3537-3550. DOI: 10.1175/JCLI-D-13-00274.1.

Collins, M., M. Botzet, A. F. Carril, et al., 2006: Interannual to Decadal Climate Predictability in the North Atlantic: A Multimodel-Ensemble Study. *J. Climate*, 19, 1195–1203. doi: http://dx.doi.org/10.1175/JCLI3654.1.

Compo, G. P., Whitaker, J. S., Sardeshmukh, P. D., et al., 2011: The Twentieth Century Reanalysis Project. *Q.J.R. Meteorol. Soc.*, 137: 1–28. doi: 10.1002/qj.776

Cunningham, S. A. and Coauthors, 2007: Temporal Variability of the Atlantic Meridional Overturning Circulation at 26.5°N. *Science*, 317(5840): 935–938. DOI:10.1126/science.1141304.

DelSole, T., and M. K. Tippett, 2007: Predictability: Recent insights from information theory, *Rev. Geophys.*, 45, RG4002, doi:10.1029/2006RG000202.

DelSole, T. and M. K. Tippett, 2009a: Average Predictability Time. Part I: Theory. *J. Atmos. Sci.*, 66, 1172–1187. doi: http://dx.doi.org/10.1175/2008JAS2868.1.

DelSole, T. and M. K. Tippett, 2009b: Average Predictability Time. Part II: Seamless Diagnoses of Predictability on Multiple Time Scales. *J. Atmos. Sci.*, 66, 1188–1204. doi:

http://dx.doi.org/10.1175/2008JAS2869.1.

DelSole, T., L. Jia, and M. K. Tippett, 2013: Decadal prediction of observed and simulated sea surface temperatures. *Geophys. Res. Lett.*, 40, 2773–2778, doi:10.1002/grl.50185.

Delworth, T., S. Manabe, and R. J. Stouffer, 1993: Interdecadal Variations of the Thermohaline Circulation in a Coupled Ocean-Atmosphere Model. *J. Climate*, 6, 1993–2011. doi: http://dx.doi.org/10.1175/1520-0442(1993)006<1993:IVOTTC>2.0.CO;2.

Delworth, T., and F. Zeng, 2012: Multicentennial variability of the Atlantic meridional overturning circulation and its climatic influence in a 4000 year simulation of the GFDL CM2.1 climate model, *Geophys. Res. Lett.*, 39, L13702, doi:10.1029/2012GL052107.

Deser, C., M. A. Alexander, and M. S. Timlin, 2003: Understanding the Persistence of Sea Surface Temperature Anomalies in Midlatitudes. *J. Climate*, 16, 57–72. doi: http://dx.doi.org/10.1175/1520-0442(2003)016<0057:UTPOSS>2.0.CO;2.

Deser, C., G. Magnusdottir, R. Saravanan, and A. Phillips, 2004: The effects of North Atlantic SST and sea ice anomalies on the winter circulation in CCM3. Part II: Direct and indirect components of the response. *J. Climate*, 17, 877–889. doi: http://dx.doi.org/10.1175/1520-0442(2004)017<0857:TEONAS>2.0.CO;2.

Enfield, D.B., A.M. Mestas-Nunez, and P.J. Trimble, 2001: The Atlantic Multidecadal Oscillation and its relationship to rainfall and river flows in the continental U.S., *Geophys. Res. Lett.*, 28: 2077-2080.

Flato, G., et al. 2013: Evaluation of Climate Models. In: *Climate Change 2013: The Physical Science Basis. Contribution of Working Group I to the Fifth Assessment Report of the*

Intergovernmental Panel on Climate Change [Stocker, T.F., D. Qin, G.-K. Plattner, M. Tignor, S.K. Allen, J. Boschung, A. Nauels, Y. Xia, V. Bex and P.M. Midgley (eds.)]. Cambridge University Press, Cambridge, United Kingdom and New York, NY, USA.

Jia, L. and T. DelSole, 2011: Diagnosis of Multiyear Predictability on Continental Scales. *J. Climate*, 24, 5108–5124. doi: http://dx.doi.org/10.1175/2011JCLI4098.1.

Jia, L., and T. DelSole, 2013: Multi-year predictability of temperature and precipitation in multiple climate models. *Geophys. Res. Lett.*, 39, L17705, doi:10.1029/2012GL052778.

Kaplan, A., M. Cane, Y. Kushnir, et al., 1998: Analyses of global sea surface temperature 1856-1991. *J. Geophys. Res.*, 103, 18, 567-18, 589.

Kerr, R. A., 2000, A North Atlantic climate pacemaker for the centuries. *Science*, 288 (5473), 1984-1986.

Knight, J. R., R. J. Allan, C. K. Folland, M. Vellinga, and M. E. Mann, 2005, A signature of persistent natural thermohaline circulation cycles in observed climate. *Geophys. Res. Lett.*, 32, L20708, doi:10.1029/2005GL024233.

Latif, M., M. Collins, H. Pohlmann, and N. Keenlyside, 2006: A Review of Predictability Studies of Atlantic Sector Climate on Decadal Time Scales. *J. Climate*, 19, 5971–5987. doi: http://dx.doi.org/10.1175/JCLI3945.1.

Latif, M., T. Martin, and W. Park, 2013: Southern Ocean Sector Centennial Climate Variability and Recent Decadal Trends. *J. Climate*, 26, 7767–7782. doi: org/10.1175/JCLI-D-12-00281.1.

Lorenz E. N., 1963: Deterministic Nonperiodic Flow. *J. Atmos. Sci.*, 20, 130–141. doi: http://dx.doi.org/10.1175/1520-0469(1963)020<0130:DNF>2.0.CO;2.

Lorenz E.N., 1975: The physical bases of climate and climate modelling. In: Climate predictability number 16 in GARP Publication Series 132–136. WMO, Switzerland.

Lumpkin R. and K. Speer, 2003: Large-Scale Vertical and Horizontal Circulation in the North Atlantic Ocean. *J. Phys. Oceanogr.*, 33, 1902–1920.doi: http://dx.doi.org/10.1175/1520-0485(2003)033<1902:LVAHCI>2.0.CO;2.

Madec, G., 2008: NEMO reference manual, ocean dynamics component: NEMO-OPA. Preliminary version, Note Pole Model. 27, Inst. PierreSimon Laplace, Paris.

Mantua N. J., S. R. Hare, Y. Zhang, et al., 1997: A Pacific Interdecadal Climate Oscillation with Impacts on Salmon Production. *Bull. Amer. Meteor. Soc.*, 78, 1069–1079. doi: http://dx.doi.org/10.1175/1520-0477(1997)078<1069:APICOW>2.0.CO;2.

Martin, T., W. Park, and M. Latif, 2013: Multi-Centennial Variability Controlled by Southern Ocean Convection in the Kiel Climate Model. *Clim. Dyn.*, 40(7), 2005-2022, doi:10.1007/s00382-012-1586-7.

Meehl, G. A., L. Goddard, J. Murphy, et al., 2009: Decadal Prediction. *Bull. Amer. Meteor. Soc.*, 90, 1467–1485. doi: http://dx.doi.org/10.1175/2009BAMS2778.1.

Park, W., and M. Latif, 2008: Multidecadal and multicentennial variability of the meridional overturning circulation. *Geophys. Res. Lett.*, 35, L22703, doi:10.1029/2008GL035779.

Park W., N. Keenlyside, M. Latif, et al., 2009: Tropical Pacific Climate and Its Response to

Global Warming in the Kiel Climate Model. *J. Climate*, 22, 71–92. doi: http://dx.doi.org/10.1175/2008JCLI2261.1.

Park, W., and M. Latif, 2010: Pacific and Atlantic Multidecadal Variability in the Kiel Climate Model. *Geophys. Res. Lett.*, 37, L24702, doi:10.1029/2010GL045560.

Pohlmann H., F. Sienz, and M. Latif, 2006: Influence of the Multidecadal Atlantic Meridional Overturning Circulation Variability on European Climate. *J. Climate*, 19, 6062–6067. doi: http://dx.doi.org/10.1175/JCLI3941.1.

Rayner, N. A., D. E. Parker, E. B. Horton, et al., 2003: Global analyses of sea surface temperature, sea ice, and night marine air temperature since the late nineteenth century. *J. Geophys. Res.*, 108, D14, 4407, doi: 10.1029/2002JD002670.

Roeckner, E., et al., 2003: The atmospheric general circulation model ECHAM5. Part I: Model description, Rep. 349, 127 pp., Max Planck Inst. for Meteorol., Hamburg, Germany.

Taylor, K. E., R. J. Stouffer, and G. A. Meehl, 2012: An Overview of CMIP5 and the Experiment Design. *Bull. Amer. Meteor. Soc.*, 93, 485–498. doi: http://dx.doi.org/10.1175/BAMS-D-11-00094.1.

Van der Swaluw, E., S. S. Drijfhout, and W. Hazeleger, 2007: Bjerknes Compensation at High Northern Latitudes: The Ocean Forcing the Atmosphere. *J. Climate*, 20, 6023–6032. doi: http://dx.doi.org/10.1175/2007JCLI1562.1.

Wang, C., et al., 2014: A global perspective on CMIP5 climate model biases. *Nature Climate*

Change, 4, 201–205 (2014). doi:10.1038/nclimate2118

Yang, X., et al., 2013: A Predictable AMO-Like Pattern in the GFDL Fully Coupled Ensemble Initialization and Decadal Forecasting System. *J. Climate*, 26, 650–661. doi: http://dx.doi.org/10.1175/JCLI-D-12-00231.1.

Figure Captions:

Fig. 1 Climatological annual mean of selected variables derived from the control simulation with the KCM. a) Barotropic stream function (Sv, $1Sv=10^6 m^3/s$), b) overturning stream function in the Atlantic basin (Sv), c) mixed layer depth (m), and d) sea ice concentration. The last 4,200 years have been used for the calculation.

Fig. 2 Spatial pattern of potential predictability variance fraction for pentadal (upper panels), decadal (middle panels) and 25-year means (lower panels) obtained from the KCM (left), and CMIP5 ensemble (right). Areas shown in red are significant at 95% confidence level according to an F-test.

Fig. 3 The most predictable component of surface air temperature (SAT) in the Northern Hemisphere in the KCM. a) Spatial pattern, b) the corresponding time series that is normalized, c) the power spectrum (blue line), where the red lines indicate the 95% (red solid line) and 90% (red dashed line) confidence level, respectively.

Fig. 4 Composites (positive composite-negative composite) of a) SST (K), b) ocean heat flux convergence (W/m^2) in the upper 273 meters, c) net heat flux (W/m^2), d) the residual part of the heat budget (W/m^2) using the APT1 time series as an index and one standard deviation as thresholds (see Fig. 3b). Positive heat flux means warming of the ocean. Areas shown in color are significant at the 95% level according to a t-test.

Fig. 5 Composites (positive composite-negative composite) of a) the barotropic stream function and b) sea ice concentration (varying between 0 and ±1) using the APT1 time series as an index and one standard deviation as thresholds (see Fig. 3b). Areas shown in color are significant at the 95% level according to a t-test.

Fig. 6 The second most predictable component of surface air temperature (SAT) in the Northern Hemisphere in the KCM. a) Spatial pattern, b) the corresponding time series that is normalized, c) the power spectrum (blue line), where the red lines indicate the 95% (red solid line) and 90% (red dashed line) confidence level, respectively.

Fig. 7 Composites (positive composite-negative composite) of a) SST (K), b) ocean heat flux convergence (W/m^2) in upper 273 meters, c) net heat flux (W/m^2), d) the residual part of the heat budget (W/m^2) using the APT2 time series an index and one standard deviation as thresholds (see Fig. 6b) Areas shown in color are significant at 95% level from a t-test.

Fig. 8 Regression of monthly ocean temperature anomalies averaged in (145°-165°E, 40°-45°N) upon APT2 time series in the KCM. Negative lags mean APT2 lags ocean temperature.

Fig. 9 Spatial patterns of a) APT1 and b) APT2 calculated from surface air temperature (SAT) of the CMIP5 ensemble. The total length of the concatenated time series amounts to 5,100 years (see section 2).

Fig. 10 Projections of SAT from the 20th Century Reanalysis data onto a) APT1 and b) APT2 (red lines) of the KCM. The black lines are the observed AMO index and PDO index, respectively. All time series are normalized.

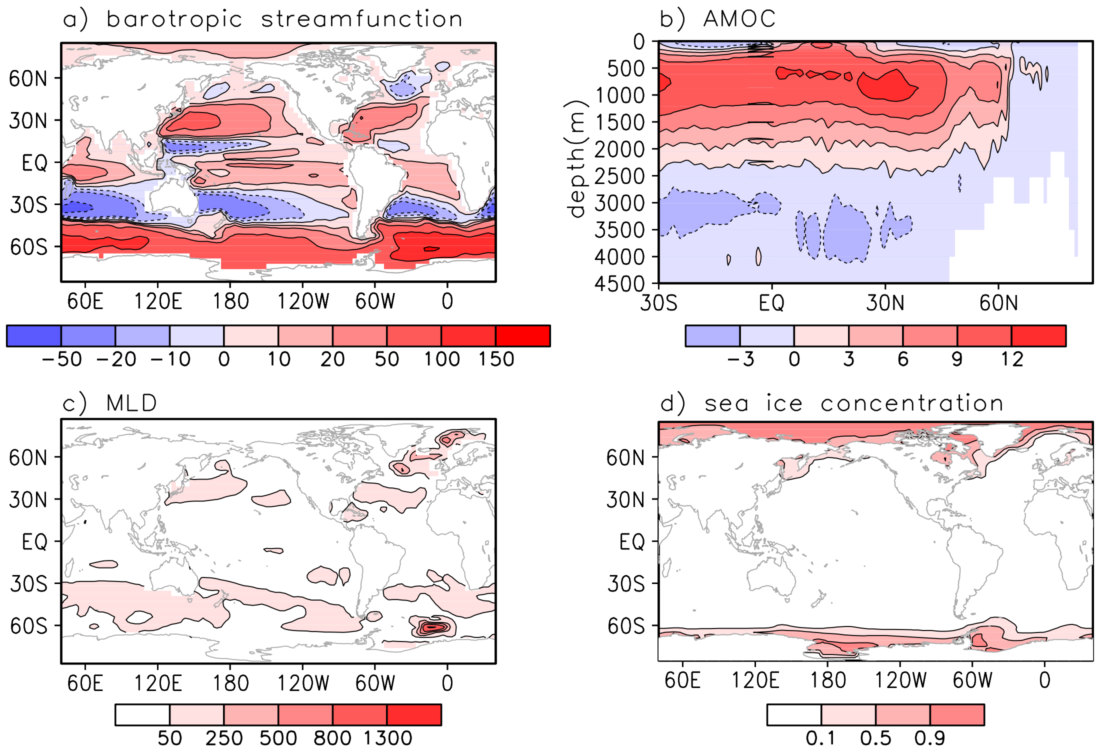

Fig. 1 Climatological annual mean of selected variables derived from the control simulation with the KCM. a) Barotropic stream function (Sv, 1Sv=10^6m^3/s), b) overturning stream function in the Atlantic basin (Sv), c) mixed layer depth (m), and d) sea ice concentration. The last 4,200 years have been used for the calculation.

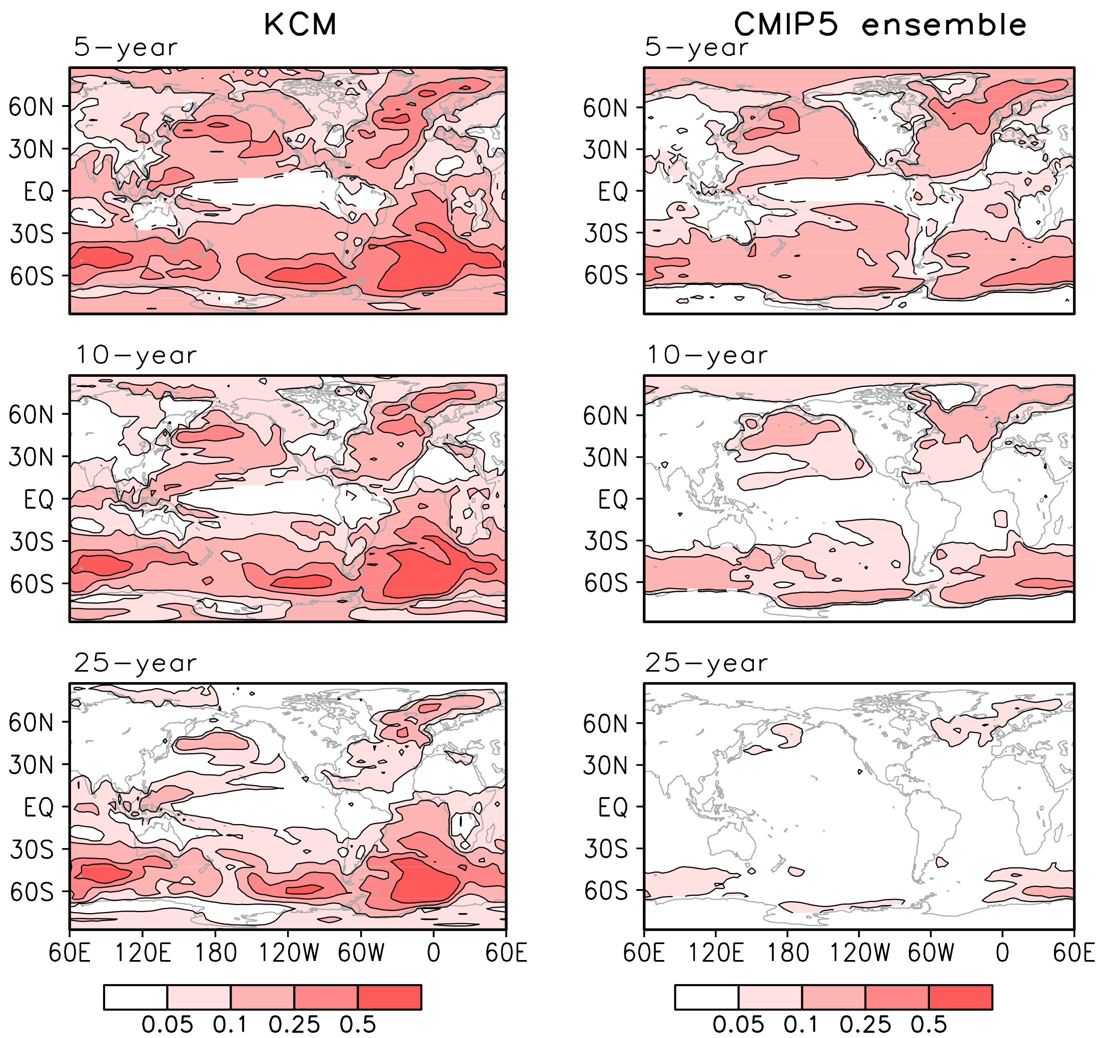

Fig. 2 Spatial pattern of potential predictability variance fraction for pentadal (upper panels), decadal (middle panels) and 25-year means (lower panels) obtained from the KCM (left), and CMIP5 ensemble (right). Areas shown in red are significant at 95% confidence level according to an F-test.

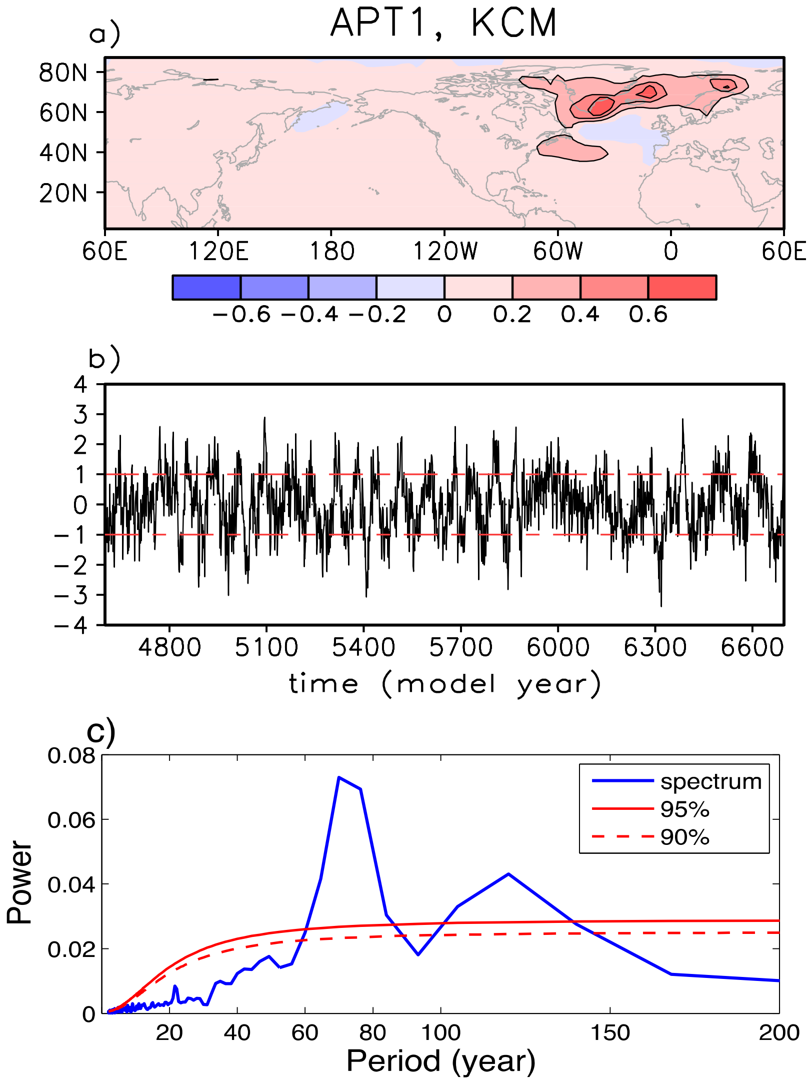

Fig. 3 The most predictable component of surface air temperature (SAT) in the Northern Hemisphere in the KCM. a) Spatial pattern, b) the corresponding time series that is normalized, c) the power spectrum (blue line), where the red lines indicate the 95% (red solid line) and 90% (red dashed line) confidence level, respectively.

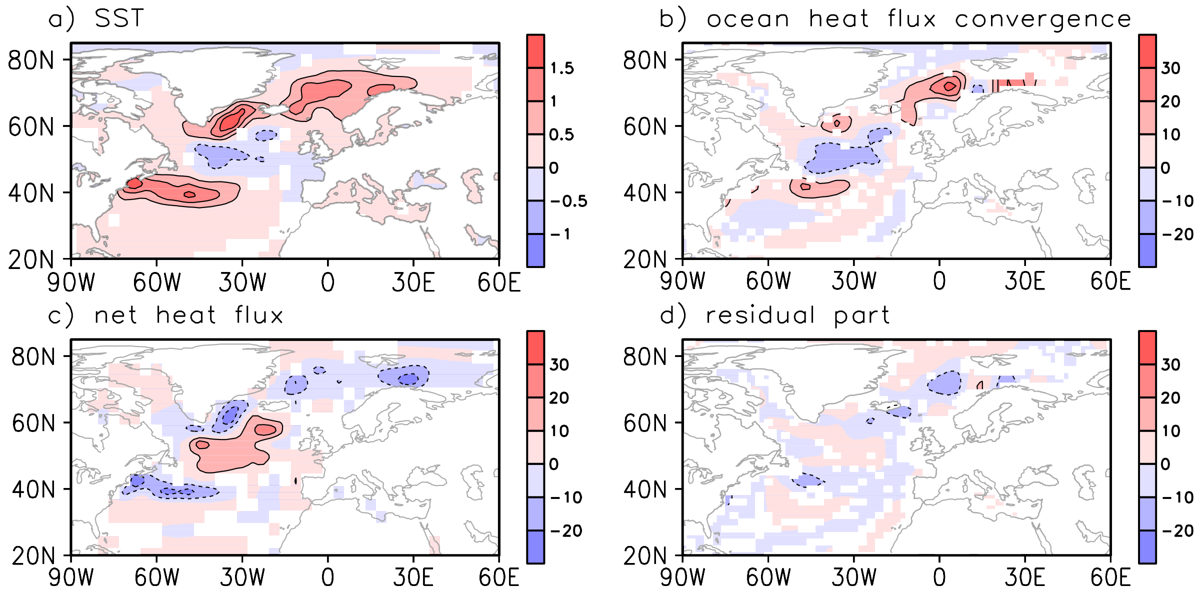

Fig. 4 Composites (positive composite-negative composite) of a) SST (K), b) ocean heat flux convergence (W/m^2) in the upper 273 meters, c) net heat flux (W/m^2), d) the residual part of the heat budget (W/m^2) using the APT1 time series as an index and one standard deviation as thresholds (see Fig. 3b). Positive heat flux means warming of the ocean. Areas shown in color are significant at the 95% level according to a t-test.

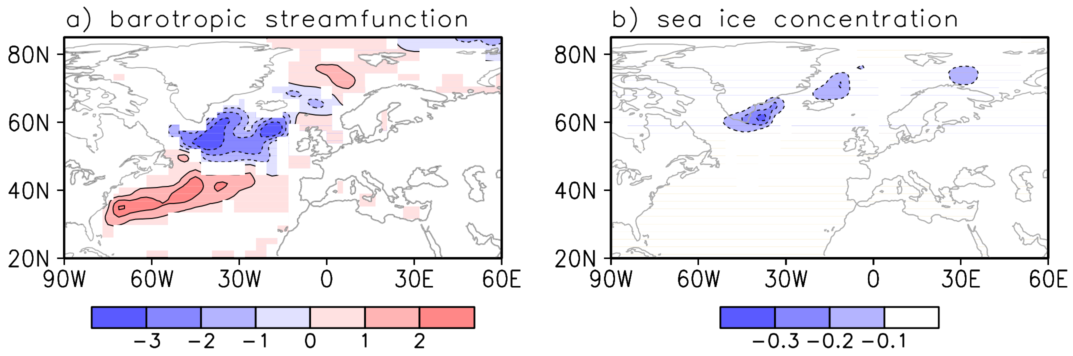

Fig. 5 Composites (positive composite-negative composite) of a) the barotropic stream function and b) sea ice concentration (varying between 0 and ±1) using the APT1 time series as an index and one standard deviation as thresholds (see Fig. 3b). Areas shown in color are significant at the 95% level according to a t-test.

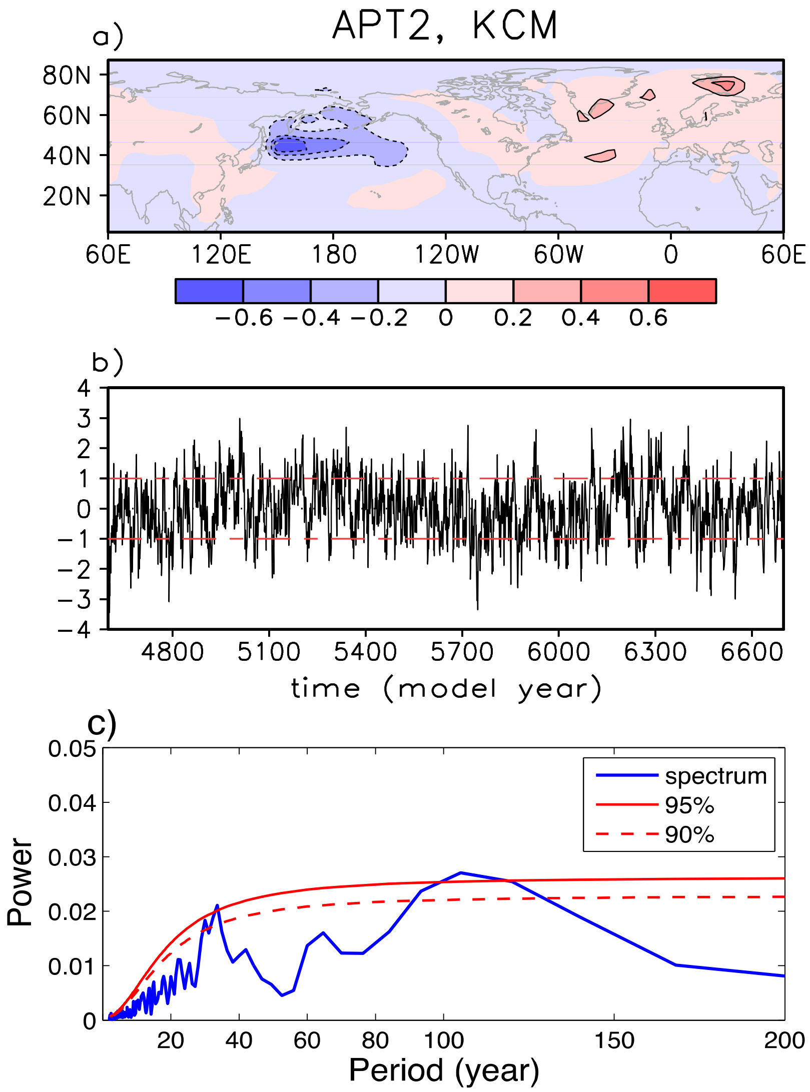

Fig. 6 The second most predictable component of surface air temperature (SAT) in the Northern Hemisphere in the KCM. a) Spatial pattern, b) the corresponding time series that is normalized, c) the power spectrum (blue line), where the red lines indicate the 95% (red solid line) and 90% (red dashed line) confidence level, respectively.

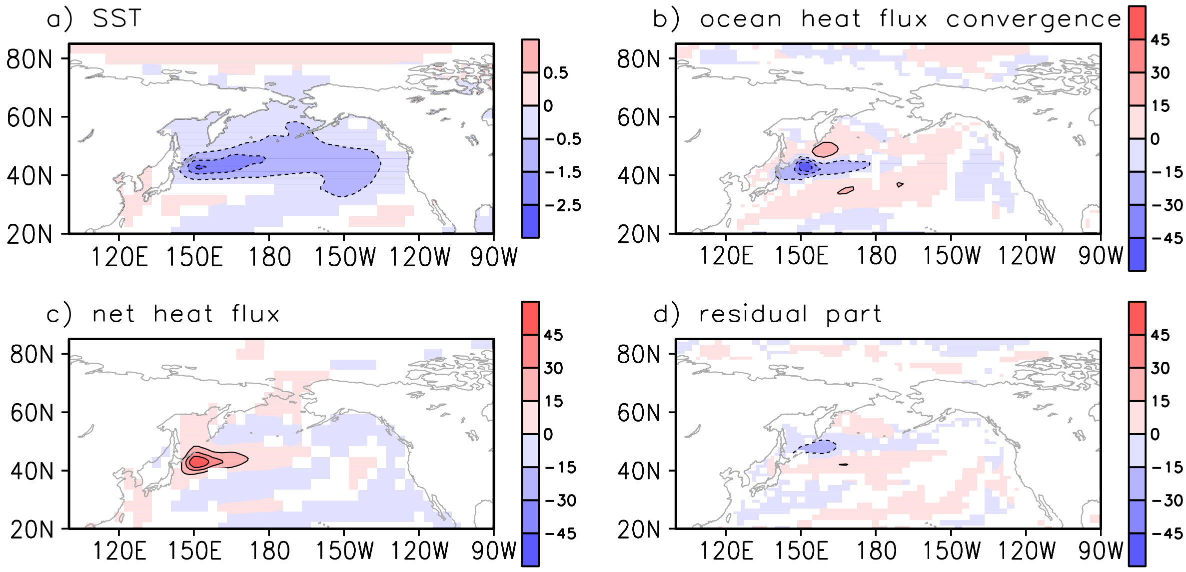

Fig. 7 Composites (positive composite-negative composite) of a) SST (K), b) ocean heat flux convergence (W/m^2) in upper 273 meters, c) net heat flux (W/m^2), d) the residual part of the heat budget (W/m^2) using the APT2 time series an index and one standard deviation as thresholds (see Fig. 6b) Areas shown in color are significant at 95% level from a t-test.

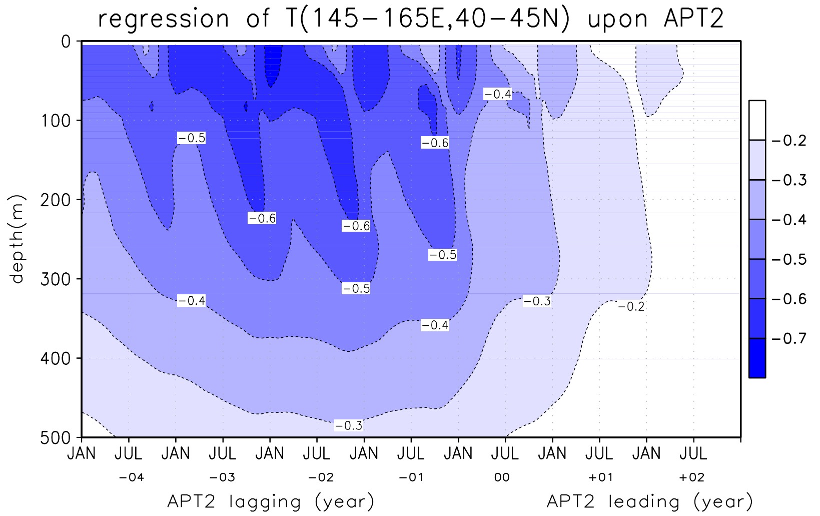

Fig. 8 Regression of monthly ocean temperature anomalies averaged in (145°-165°E, 40°-45°N) upon APT2 time series in the KCM. Negative lags mean APT2 lags ocean temperature.

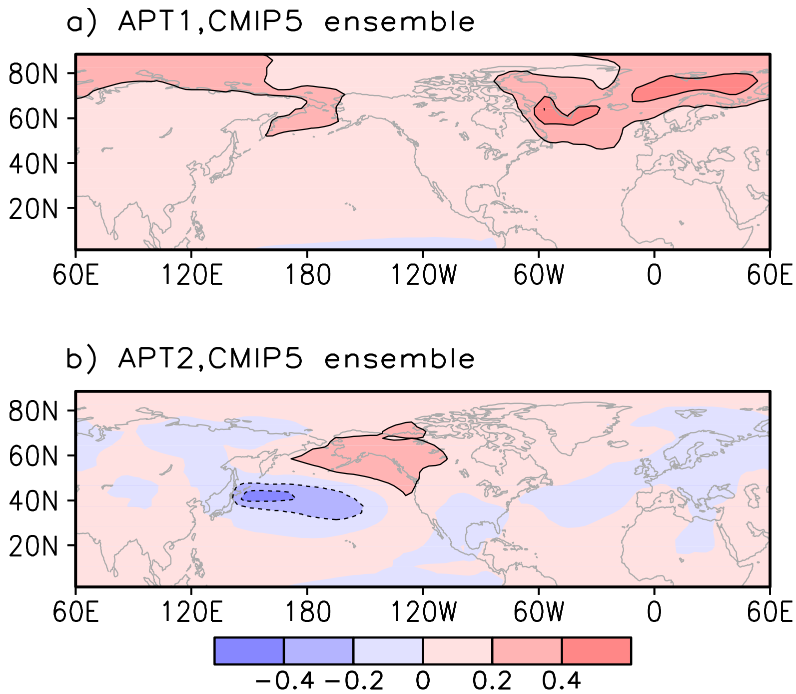

Fig. 9 Spatial patterns of a) APT1 and b) APT2 calculated from surface air temperature (SAT) of the CMIP5 ensemble. The total length of the concatenated time series amounts to 5,100 years (see section 2).

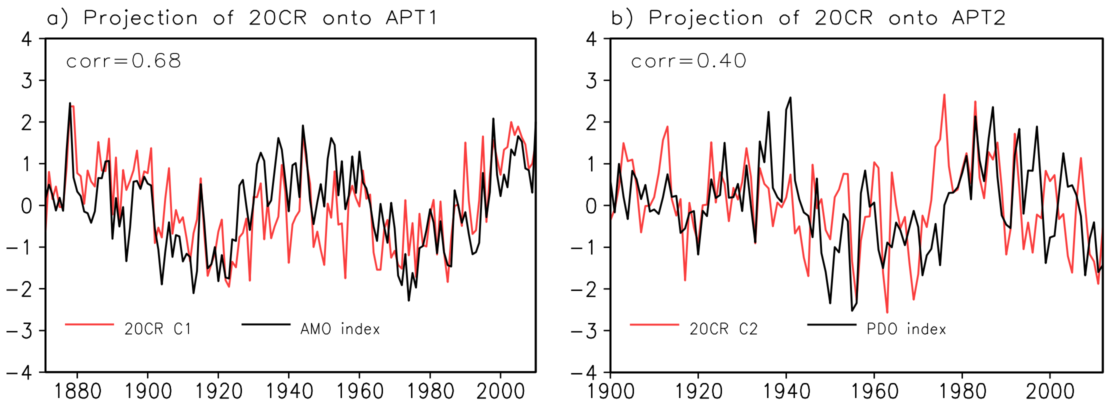

Fig. 10 Projections of SAT from the 20 th Century Reanalysis data onto a) APT1 and b) APT2 (red lines) of the KCM. The black lines are the observed AMO index and PDO index, respectively. All time series are normalized.